

# Greatly enhanced light emission of MoS<sub>2</sub> using photonic crystal heterojunction

Liu Jiang-tao<sup>1,2,3\*</sup>, Tong Hong<sup>1</sup>, Wu Zhen-Hua<sup>4</sup>, Huang Jin-Bao<sup>1</sup>, Zhou Yun-Song<sup>5†</sup>

<sup>1</sup>College of Mechanical and electrical engineering, Guizhou Minzu University, Guiyang 550025, China

<sup>2</sup>Department of Physics, Nanchang University, Nanchang 330031, China

<sup>3</sup>Institute for Advanced Study, Nanchang University, Nanchang 330031, China

<sup>4</sup>Key Laboratory of Microelectronic Devices and Integrated Technology, Institute of Microelectronics, Chinese Academy of Sciences, Beijing 100029, China

<sup>5</sup>Department of Physics, Capital Normal University, Beijing 100037, China

\*Email: jtliu@semi.ac.cn † Email: 263zys@263.net

October 13, 2018

## Abstract

We study the effect of one-dimensional (1D) photonic crystal heterojunction (h-PhC) on the light absorption and light emission of monolayer molybdenum disulfide (MoS<sub>2</sub>), and obtained the analytical solution of the light absorption and emission of two-dimensional materials in 1D h-PhC. Simultaneously enhancing the light absorption and emission of the medium in multiple frequency ranges is easy as h-PhC has more models of photon localization than the common photonic crystal. Result shows that h-PhC can simultaneously enhance the light absorption and emission of MoS<sub>2</sub> and enhance the photoluminescence spectrum of MoS<sub>2</sub> by 2-3 orders of magnitude.

Two-dimensional (2D) transition metal dichalcogenides (TMDCs), such as MoS<sub>2</sub> and WSe<sub>2</sub>, are direct-gap semiconductor 2D materials with excellent optical properties and are thus considered the best materials for future optoelectronic devices[1–7]. The light absorption and emission of 2D TMDCs per unit mass are much higher than that of traditional semiconductor materials. 2D TMDCs typically have a thickness of less than 1 nm, and their light absorption and emission are weak, thus limiting their application in optoelectronic devices. However, benefit from thin thickness of 2D materials, 2D TMDCs can be combined with optical microstructures, such as photonic crystals, microcavities, and surface plasmas, and then enhance their light absorption[8–30] and emission[8, 9, 31–40] due to the optical localization in these structures. Lien et al. [8] and Serkan et al. [9] used surface plasmas or optical multilayers to enhance the light absorption and emission of MoS<sub>2</sub> or WSe<sub>2</sub>, thus enhancing the photoluminescence (PL) of MoS<sub>2</sub> or WSe<sub>2</sub> by 10-30 times.

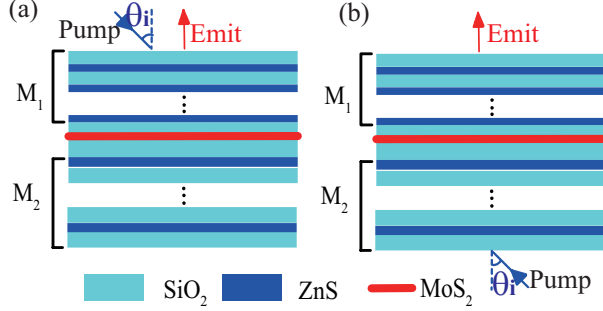


Figure 1: Schematic of h-PhC structure. (a) pump light and outgoing light on the same side; (b) pump light and outgoing light on different sides.

To further enhance the light emission and absorption of 2D TMDCs, we investigated the effect of photonic crystal heterojunction (h-PhC) on the light absorption and emission of MoS<sub>2</sub>. Similar to the semiconductor heterojunction, h-PhC comprises photonic crystals (PhC) with different lattice constants or shapes[41]. Earlier studies have found that h-PhC that comprise different PhCs can obtain strong light localization in several frequency ranges[41, 42]. On the basis of these findings, one can place h-PhC that are formed by different PhCs at intervals to form a multimode high-speed optical waveguide.

Thus, if 2D TMDCs are combined with h-PhC, the strong light localization of h-PhC in multiple frequency ranges can simultaneously enhance the light emission and absorption of 2D TMDCs. We therefore conducted a detailed study. h-PhC consists of 1D PhCs with two kinds of crystal lattices that form an h-PhC microcavity structure. To thoroughly understand the light absorption and emission in h-PhC, we first identified the analytical solution of the light absorption and emission of MoS<sub>2</sub> in h-PhC. The findings indicate that h-PhC can enhance the light absorption and emission of MoS<sub>2</sub> and enhance the PL spectrum of MoS<sub>2</sub> by 2-3 orders of magnitude, which has a promising prospect and important application value in fluorescent probe, 2D LED, etc. The analytical solution can be used not only for the light absorption and emission in h-PhC but also for the calculation of other 1D PhC-2D materials composite structures.

## Model and theory

The structure of h-PhC is shown in Fig. 1, i.e.,  $(A_1B_1)^{N_1}C_1MC_2(B_2A_2)^{N_2}$  structure.  $(A_1B_1)^{N_1}$  and  $(B_2A_2)^{N_2}$  layers constitute the two distributed Bragg reflectors (DBRs), and  $N_1$  and  $N_2$  are the numbers of cycles. The  $A_1$  and  $A_2$  layers are made of SiO<sub>2</sub>, and the refractive index  $n_{SiO_2} = 1.4923 + 0.81996\lambda^2 / (\lambda^2 - 0.10396^2) - 0.01082\lambda^2$  [43].  $\lambda' = \lambda \times 10^6$ ,  $\lambda$  is wavelength of the input light beams, and the thicknesses of the  $A_1$  and  $A_2$  layers are  $\lambda_{10}/(4 \times 1.53)$  and  $\lambda_{20}/(4 \times 1.53)$ , respectively.  $\lambda_{10}$  and  $\lambda_{20}$  is the center wavelength of the the upside PhC and the bottom PhC, respectively.  $B_1$  and  $B_2$  layers

are composed of ZnS. The refractive index  $n_{ZnS} = 8.393 + 0.14383/(\lambda^2 - 0.2421^2) + 4430.99/(\lambda^2 - 36.72^2)$  [44]. The thicknesses of the  $B_1$  and  $B_2$  layers are  $\lambda_{20}/(4 \times 2.4)$  and  $\lambda_{20}/(4 \times 2.4)$ . The  $C_1$  and  $C_2$  layers are made of SiO<sub>2</sub>, and their thicknesses are  $d_{C_1}$  and  $d_{C_2}$ , respectively. The M layer is the MoS<sub>2</sub> layer. Its thickness is 0.65 nm.

To model the absorption of MoS<sub>2</sub> in this structure, the transfer matrix method is used first [21, 45]. In the  $l$ th layer, the electric field of the TE mode light beam with incident angle  $\theta_i$  is given by

$$\mathbf{E}_l(x, y) = \left[ A_l e^{ik_x(x-x_l)} + B_l e^{-ik_x(x-x_l)} \right] e^{ik_y y} \mathbf{e}_z, \quad (1)$$

where  $k_l = k_{lx} + ik_{ly}$  is the wave vector of the incident light,  $\mathbf{e}_z$  is the unit vectors in the z direction, and  $x_l$  is the position of the  $l$ th layer in the x direction. And the magnetic field of the TM mode in the  $l$ th layer is given by

$$\mathbf{H}_l(x, y) = \left[ A_l e^{ik_x(x-x_l)} + B_l e^{-ik_x(x-x_l)} \right] e^{ik_y y} \mathbf{e}_z, \quad (2)$$

The electric (magnetic) fields of TE (TM) mode in the  $(l+1)$ th and  $l$ th layer are related by the matrix utilizing the boundary condition

$$\begin{aligned} \begin{pmatrix} A_{l+1} \\ B_{l+1} \end{pmatrix} &= \begin{pmatrix} \frac{\gamma_l + \gamma_{l+1}}{2\gamma_{l+1}} e^{ik_x d_l} & \frac{\gamma_{l+1} - \gamma_l}{2\gamma_{l+1}} e^{-ik_x d_l} \\ \frac{\gamma_{l+1} - \gamma_l}{2\gamma_{l+1}} e^{ik_x d_l} & \frac{\gamma_l + \gamma_{l+1}}{2\gamma_{l+1}} e^{-ik_x d_l} \end{pmatrix} \begin{pmatrix} A_l \\ B_l \end{pmatrix} \\ &= T^{l+1 \leftarrow l} \begin{pmatrix} A_l \\ B_l \end{pmatrix}, \end{aligned} \quad (3)$$

where  $\gamma_l = \frac{k_{lx}^r + ik_{ly}^i}{\mu_l(\omega)}$  ( $\gamma_l = \frac{k_{lx}^r + ik_{ly}^i}{\varepsilon_l(\omega)}$ ) for TE (TM) mode,  $\mu_l(\omega)$  is the permeability,  $\varepsilon_l(\omega) = \varepsilon_l^r(\omega) + i\varepsilon_l^i(\omega)$  is the complex dielectric permittivity, and  $d_l$  is the thickness of the  $l$ th layer. Thus, the fields in the  $(l+1)$ th layer are related to the incident fields by the transfer matrix

$$\begin{pmatrix} A_{l+1} \\ B_{l+1} \end{pmatrix} = T^{l+1 \leftarrow l} \dots T^{2 \leftarrow 1} T^{1 \leftarrow 0} \begin{pmatrix} A_0 \\ B_0 \end{pmatrix} = \begin{pmatrix} T_{11} & T_{12} \\ T_{21} & T_{22} \end{pmatrix} \begin{pmatrix} A_0 \\ B_0 \end{pmatrix}. \quad (4)$$

To thoroughly describe the light absorption and emission of MoS<sub>2</sub> in h-PhC, improve the computational speed to optimize the structure, and help scholars who are not familiar with the transfer matrix method for computing, we obtained the analytical solution of the light absorption and emission of MoS<sub>2</sub> in h-PhC using the transfer matrix method. Since the transfer matrix of the electric fields of TE mode and the transfer matrix of magnetic fields of TM mode have the same form, we only shows the analytical solution of the TE mode. First, for a N-period PhC in air, the transfer matrix can be write as[46]

$$\begin{pmatrix} A_0 \\ B_0 \end{pmatrix} = M_N \begin{pmatrix} A_{l+1} \\ B_{l+1} \end{pmatrix} = \begin{bmatrix} 1/t_N & r_N^*/t_N^* \\ r_N/t_N & 1/t_N^* \end{bmatrix} \begin{pmatrix} A_{l+1} \\ B_{l+1} \end{pmatrix}, \quad (5)$$

where  $\frac{1}{t_N} = \frac{1}{t_0} \frac{\sin N\beta}{\sin \beta} - \frac{\sin(N-1)\beta}{\sin \beta}$ ,  $\frac{r_N}{t_N} = \frac{r_0}{t_0} \frac{\sin N\beta}{\sin \beta}$ ,  $\beta$  is the Bloch phase in each period,  $t_0$  and  $r_0$  is the transmission amplitude and reflection amplitude of the

each period [46]. For the upper part PhC in the h-PhC, the right hand side is not air. By multiplying the transfer matrix of PhC to the C<sub>1</sub> layer  $T^{C\leftarrow P}(d_c = 0)$  and the inverse transfer matrix of PhC to the air layer  $[T^{air\leftarrow P}(d_c = 0)]^{-1}$ , we can get the transfer matrix of the upper part PhC

$$\begin{aligned} (M'_{N_1}) &= \left\{ M_{N_1} T^{C\leftarrow P}(d_c = 0) [T^{air\leftarrow P}(d_c = 0)]^{-1} \right\}^{-1} \\ &= \frac{1}{2} \begin{pmatrix} \zeta/t_{N_1} + \zeta' r'_{N_1}/t'_{N_1} & \zeta' t_{N_1} + \zeta r'_{N_1}/t'_{N_1} \\ \zeta r'_{N_1}/t'_{N_1} + \zeta'/t'_{N_1} & \zeta' r'_{N_1}/t'_{N_1} + \zeta/t'_{N_1} \end{pmatrix} \\ &= \begin{bmatrix} 1/t'_{N_1} & r'_{N_1}/t'_{N_1} \\ r'_{N_1}/t'_{N_1} & 1/t'_{N_1} \end{bmatrix}, \end{aligned} \quad (6)$$

where  $\zeta = 1 + \sqrt{\varepsilon_c} \cos \theta_c$ ,  $\zeta' = 1 - \sqrt{\varepsilon_c} \cos \theta_c$ ,  $\varepsilon_c = \varepsilon_{c_1} = \varepsilon_{c_2}$  is the refractive index of C<sub>1</sub> and C<sub>2</sub> layers,  $\theta_c = \theta_{c_1} = \theta_{c_2}$  is the propagation angle in the C<sub>1</sub> and C<sub>2</sub> layer. Similar, we can get the transfer matrix of the lower part PhC,

$$\begin{aligned} M'_{N_2} &= \left\{ [T^{C\leftarrow P}(d_c = 0)]^{-1} T^{air\leftarrow E}(d_c = 0) \right\} M_{N_2} = \\ &= \frac{1}{2} \begin{pmatrix} \zeta/t_{N_2} + \zeta' r'_{N_2}/t'_{N_2} & \zeta'/t'_{N_2} + \zeta r'_{N_2}/t'_{N_2} \\ \zeta r'_{N_2}/t'_{N_2} + \zeta'/t'_{N_2} & \zeta' r'_{N_2}/t'_{N_2} + \zeta/t'_{N_2} \end{pmatrix} \\ &= \begin{bmatrix} 1/t'_{N_2} & r'_{N_2}/t'_{N_2} \\ r'_{N_2}/t'_{N_2} & 1/t'_{N_2} \end{bmatrix}. \end{aligned} \quad (7)$$

The transfer matrix of the C<sub>1</sub> layer is [11]

$$M_f(d_{C_1}) = \begin{bmatrix} e^{-ik_{cx}d_{C_1}} & 0 \\ 0 & e^{ik_{cx}d_{C_1}} \end{bmatrix}, \quad (8)$$

and the transfer matrix of the C<sub>2</sub> layer is

$$M_f(L_{cav} - d_{C_1}) = \begin{bmatrix} e^{-ik_{cx}(L_{cav} - d_{C_1})} & 0 \\ 0 & e^{ik_{cx}(L_{cav} - d_{C_1})} \end{bmatrix}, \quad (9)$$

where  $L_{cav} = d_{C_1} + d_{C_2}$  is the microcavity length,  $k_{cx}$  wave vector of the light in the C<sub>1</sub> or C<sub>2</sub> layer. Take the approximate  $e^{ik_{Mx}d_M} \approx 1 + ik_{Mx}d_M$ , where  $k_{Mx}$  wave vector of the light in the MoS<sub>2</sub> layer and  $d_M$  is the thickness of the and MoS<sub>2</sub> layer, the transfer matrix of the MoS<sub>2</sub> layer is

$$M_{MoS_2} = [T^{C\leftarrow MoS_2} T^{MoS_2\leftarrow C}(d = 0)]^{-1} = \begin{bmatrix} 1 - \eta_1 & -\eta_2 \\ \eta_2 & 1 + \eta_1 \end{bmatrix}, \quad (10)$$

where  $\eta_1 = ik_{Mx}d_M \left[ \left( \sqrt{\varepsilon_{MoS_2}/\varepsilon_C} \cos \theta_{MoS_2} / \cos \theta_c \right) + \left( \sqrt{\varepsilon_c/\varepsilon_{MoS_2}} \cos \theta_c / \cos \theta_{MoS_2} \right) \right] / 2$ ,

and  $\eta_2 = ik_{Mx}d_M \left[ \left( \sqrt{\varepsilon_{MoS_2}/\varepsilon_C} \cos \theta_{MoS_2} / \cos \theta_c \right) - \left( \sqrt{\varepsilon_c/\varepsilon_{MoS_2}} \cos \theta_c / \cos \theta_{MoS_2} \right) \right] / 2$ .

Thus, the total transfer matrix of the C<sub>1</sub>, C<sub>2</sub>, and MoS<sub>2</sub> layer is

$$M_f(d_{C_1}) M_{MoS_2} M_f(L - d_{C_1}) = \begin{bmatrix} (1 - \eta_1) e^{-ikL} & -\eta_2 e^{ik(L - 2d_{C_1})} \\ \eta_2 e^{-ik(L - d_{C_1})} & (1 + \eta_1) e^{ikL} \end{bmatrix}. \quad (11)$$

The total transfer matrix of the h-PhC is

$$M = M'_{N_1} M_f (d_{C_1}) M_{MoS_2} M_f (L - d_{C_1}) M'_{N_2}. \quad (12)$$

we can get the matrix element

$$M_{11} = \left[ (1 - \eta_1) / \varphi_1 t'_{N_1} - \eta_2 \varphi_2 r'_{N_2} / t'_{N_1} + \eta_2 r'_{N_1} / \varphi_2 t'^*_{N_1} + (1 + \eta_1) \varphi_1 r'_{N_2} r'_{N_1} / t'^*_{N_1} \right] / t'_{N_2}, \quad (13)$$

and

$$M_{21} = \left[ (1 - \eta_1) r'_{N_1} / \varphi_1 t'_{N_1} - \eta_2 \varphi_2 r'_{N_2} r'_{N_1} / t'_{N_1} + \eta_2 / \varphi_2 t'^*_{N_1} + (1 + \eta_1) \varphi_1 r'_{N_2} / t'^*_{N_1} \right] / t'_{N_2}, \quad (14)$$

where  $\varphi_1 = e^{ikL}$ ,  $\varphi_2 = e^{ik(L-2d_{C_1})}$ . The transmittance of the h-PhC is  $T = |1/M_{11}|^2$ ; the reflectance of the h-PhC is  $R = |M_{21}/M_{11}|^2$  [11, 46]; the absorption of MoS<sub>2</sub> layer  $A_{MoS_2} = 1 - R - T$ .

The spontaneous emission of the monolayer MoS<sub>2</sub> in the h-PhC can be treated as two emitted correlated wavepackets, upward (downward) propagating wave packet  $\mathcal{P}_u$  ( $\mathcal{P}_d$ ). The emission wavepackets are partially transmitted and reflected by the two DBRs. The field amplitude of the light emitted out from the exit DBR mirror is given by [47–49]

$$\begin{aligned} E_{DBRt}(t) &= t_t \mathcal{P}(t) + t_t r_b \mathcal{P}(t - \frac{2z_{ol}}{c}) \\ &\quad + t_t (r_b r_t) \mathcal{P}(t - \frac{2L_{oc}}{c}) \\ &\quad + t_t (r_b r_b r_t) \mathcal{P}(t - \frac{2z_{ol}}{c} - \frac{2L_{oc}}{c}) + \dots, \end{aligned} \quad (15)$$

where  $r_t$  and  $t_t$  is the reflection amplitude and transmission amplitude of the exit DBR mirror, respectively,  $r_b$  is the reflection amplitude of the back DBR mirror,  $z_{ol}$  is the distance between the monolayer MoS<sub>2</sub> and back DBR mirror. When the pump and outgoing lights are on the same side of the h-PhC,  $r_t = r'_{N_1}$ ,  $t_t = t'_{N_1}$ ,  $r_b = r'_{N_2}$ ,  $z_{ol} = d_{C_2}$ ; When the pump and outgoing lights are on the different side of the h-PhC,  $r_t = r'_{N_2}$ ,  $t_t = t'_{N_2}$ ,  $r_b = r'_{N_1}$ ,  $z_{ol} = d_{C_1}$ ;  $\mathcal{P}(t)$  is the electric amplitude against time for a single emission event (in either direction),  $L_{oc} = n_c L_{cav} = n_c (d_{C_1} + d_{C_2})$  is the optical length of microcavity,  $n_c$  is the refractive index of the C<sub>1</sub> and C<sub>2</sub> layer. By using the Fourier transform, the emitted radiation from the top DBR mirror in the frequency domain can be

written as

$$\begin{aligned}
E_{DBRt}(\omega) &= \frac{t_t}{2\pi} \int_{-\infty}^{\infty} \mathcal{P}(t) \exp(i\omega t) dt \\
&+ \frac{t_t r_b}{2\pi} \int_{-\infty}^{\infty} \mathcal{P}(t - \frac{2z_{ol}}{c}) \exp(i\omega t) dt \\
&+ \frac{t_t (r_b r_t)}{2\pi} \int_{-\infty}^{\infty} \mathcal{P}(t - \frac{2L_{oc}}{c}) \exp(i\omega t) dt \\
&+ \frac{t_t (r_b r_b r_t)}{2\pi} \int_{-\infty}^{\infty} \mathcal{P}(t - \frac{2z_{ol}}{c} - \frac{2L_{oc}}{c}) \\
&\times \exp(i\omega t) dt + \dots
\end{aligned} \tag{16}$$

Neglected the changes of the spontaneous time, integral of Eq. (16), the emission intensity can be calculated by [47, 48]

$$\begin{aligned}
|E_{DBRt}(\lambda)|^2 &= \frac{1 + R_b + 2\sqrt{R_b} \cos\left(\frac{4\pi n_c Z_{OL}}{\lambda}\right)}{1 + R_b R_t - 2\sqrt{R_b R_t} \cos\left(\frac{4\pi n_c L_{cav}}{\lambda}\right)} \\
&\times T_t |\mathcal{P}(\lambda)|^2,
\end{aligned} \tag{17}$$

where  $T_t = |t_t|^2$  and  $R_t = |r_t|^2$  is the transmittance and reflectance of the exit DBR mirror, respectively,  $T_b = |t_b|^2$  and  $R_b = |r_b|^2$  is the the transmittance and reflectance of the back DBR mirror with the MoS<sub>2</sub> TFT, respectively.

## RESULTS

We first calculated the absorption and the relative radiation intensity of MoS<sub>2</sub> when the pump and outgoing lights are on the same side of the h-PhC. The calculated parameters are as follows:  $\lambda_{10} = 730$  nm,  $\lambda_{20} = 630$  nm,  $d_{C_1} = 0$  nm,  $d_{C_2} = 214$  nm,  $N_1 = 6$ , and  $N_2 = 7$ . The incident angle  $\theta_i = 48^\circ$ . The pump light is in TE mode. The outgoing light is vertically emitted. Two strong absorption peaks emerge at wavelengths of 488 (consistent with the wavelength of the pump light used in the experiment[9]) and 602 nm. Quite small difference can be found between the calculation results of the analytical solution and the transfer matrix method due to the approximate  $e^{ik_{Mx}d_M} \approx 1 + ik_{Mx}d_M$  is used. The optical wavelength of 602 nm is in the bandgap of the two PhCs with strong localization properties (upper illustration of Figure 1) and strong absorption. The absorption can reach 0.7 or more, which is approximately 6 times more than that without h-PhC. If the wavelength of the pump light is 488 nm, it is only in the bandgap of the bottom PhC. The localization is weak. The absorption is 0.4, which is about 3 times more than that without h-PhC. The emission efficiency is enhanced by 140 times due to the high reflectivity of the PhCs on both sides. Thus, when the pump lights are 488 and 602 nm, the PL is enhanced by approximately 420 and 840 times, respectively.

The MoS<sub>2</sub> absorption in h-PhC is sensitive to the incidence angle. The calculation results are shown in Figure 3. The resonant wavelength of the microcavity

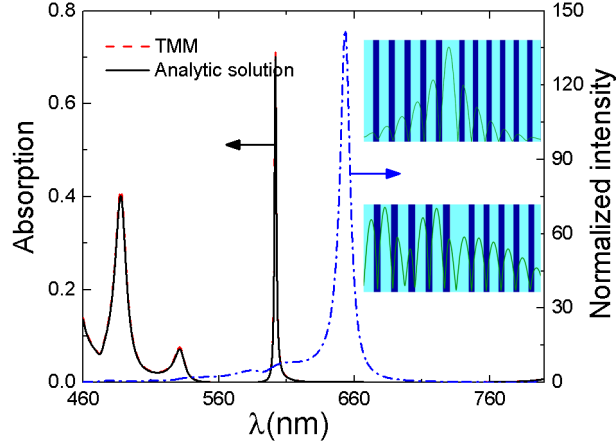


Figure 2: The absorption and relative radiation intensity of MoS<sub>2</sub> when the pump and outgoing lights are on the same side of the h-PhC. The black solid line and the red dashed line are the calculation results of the analytical solution and the transfer matrix method, respectively. The upper and lower illustrations are the light field distribution at wavelengths of 488 and 602 nm, respectively.

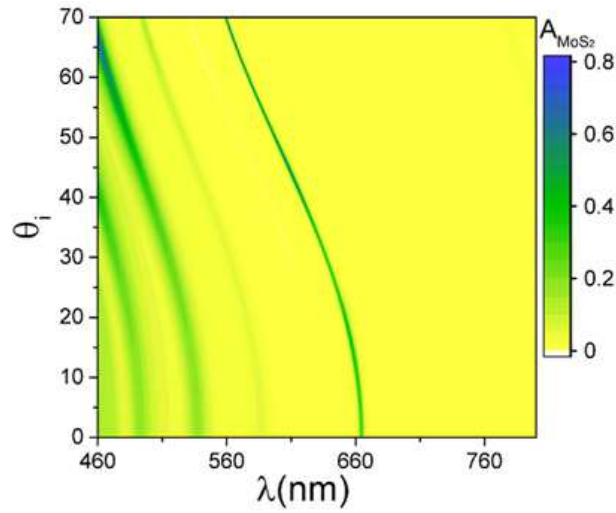


Figure 3: h-PhC MoS<sub>2</sub> absorption changes as the incident angle and wavelength change.

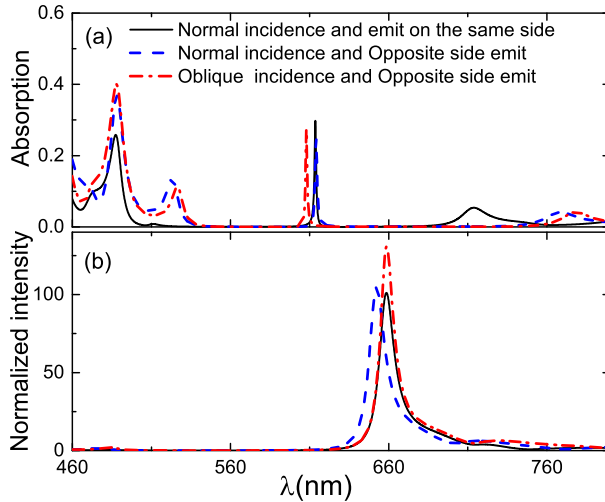


Figure 4: (a) Light absorption and (b) light emission of MoS<sub>2</sub> in h-PhC under different pump lights. The black solid line: when the pump light is normally incident, the pump and outgoing lights are in the same side of the h-PhC; the blue dashed line: when the pump light is normally incident, the pump and outgoing lights are on different sides of the h-PhC; the red dash-dotted line: when the pump light is obliquely incident, the pump and outgoing lights are on different sides of the h-PhC.

is  $m_0\lambda_c/2 = L_c\cos\theta'$ .  $L_c = n_c d_c$  is the microcavity optical path,  $m_0$  is a positive integer, and  $\theta' = \arcsin\theta_i/n_c$  is the propagation angle of light in the defective layer. Thus, when the incident angle increases, the resonance wavelength moves in the short-wave direction, the reflectivity of the PhCs on both sides increases, the travel path of light in MoS<sub>2</sub> increases, and the maximum absorption can reach 0.8 or more. PL is enhanced by approximately 3 orders of magnitude.

We also calculated the positive incidence of the pump light and the absorption and relative radiation intensity of MoS<sub>2</sub> when the pump and outgoing lights are on different sides of the h-PhC. As in the experiment, in our calculation, the wavelength of the pump light is 488 nm, and the wavelength of the outgoing light approaches 660 nm. We calculated the corresponding parameters by optimizing the h-PhC structure under different pump light incidences as follows: when the pump light is normally incident and the pump and outgoing lights are on the same side of the h-PhC,  $\lambda_{10} = 580$  nm,  $\lambda_{20} = 610$  nm,  $d_{C_1} = 2$  nm,  $d_{C_2} = 214$  nm,  $N_1 = 7$ , and  $N_2 = 7$ . When the pump light is normally incident and the pump and outgoing lights are on different sides of the h-PhC,  $\lambda_{10} = 630$  nm,  $\lambda_{20} = 570$  nm,  $d_{C_1} = 11$  nm,  $d_{C_2} = 203$  nm,  $N_1 = 7$ , and  $N_2 = 7$ . When the pump light is obliquely incident and the pump and outgoing lights are on different sides of the h-PhC,  $\lambda_{10} = 660$  nm,  $\lambda_{20} = 580$  nm,  $d_{C_1} = 0$  nm,  $d_{C_2} = 216$  nm,  $N_1 = 7$ ,  $N_2 = 7$ , and  $\theta_i = 30^\circ$ .



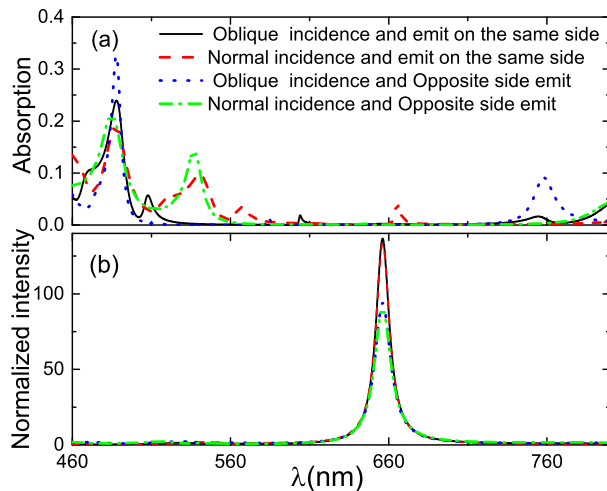


Figure 5: (a) Light absorption and (b) light emission of MoS<sub>2</sub> in homojunction PhC under different pump lights. The black solid line: when the pump light is obliquely incident and the pump and outgoing lights are on the same side; the red dashed line: when the pump light is normally incident and the pump and outgoing lights are on the same side; the blue dotted line: when the pump light is obliquely incident and the pump and outgoing lights are on different sides; the green dash-dotted line: when the pump light is normally incident and the pump and outgoing lights are on different sides.

The detailed calculation results are shown in Figure 4. Regardless of whether the pump and outgoing lights are on the same or different sides of the h-PhC, the absorption of MoS<sub>2</sub> is higher when the pump light is obliquely incident. A strong local touch in the vicinity of two wavelengths can be easily obtained as change in incidence angle can adjust the resonant wavelength. When the pump light is normally incident and the pump and outgoing lights are on different sides of the h-PhC, the absorption of MoS<sub>2</sub> is high because if MoS<sub>2</sub> in the microcavity structure obtains strong absorption and emission, the reflectivity of the rear reflector should be higher but the reflectivity of the front reflector should not be excessively high [18]. The bandgap width of the PhC is not big enough due to the large difference between the wavelengths of the pump and outgoing lights. The pump and outgoing lights on different sides realize this goal easily.

For comparison, we calculated the light absorption and emission of MoS<sub>2</sub> in a homojunction. The optimized structural parameters are as follows: when the pump light is obliquely incident and the pump and outgoing lights are on the same side,  $\lambda_{10} = \lambda_{20} = 660$  nm,  $d_{C_1} = 0$  nm,  $d_{C_2} = 215$  nm,  $N_1 = 5$ ,  $N_2 = 7$ , and  $\theta_i = 42^\circ$ . When the pump light is normally incident and the pump and outgoing lights are on the same side,  $\lambda_{10} = \lambda_{20} = 680$  nm,  $d_{C_1} = 4$  nm,  $d_{C_2} = 210$  nm,  $N_1 = 5$ , and  $N_2 = 7$ . When the pump light is obliquely incident

and the pump and outgoing lights are on different sides,  $\lambda_{10} = \lambda_{20} = 670$  nm,  $d_{C_1} = 0$  nm,  $d_{C_2} = 214$  nm,  $N_1 = 6$ ,  $N_2 = 5$ , and  $\theta_i = 54^\circ$ . When the pump light is normally incident and the pump and outgoing lights are on different sides:  $\lambda_{10} = \lambda_{20} = 650$  nm,  $d_{C_1} = 0$  nm,  $d_{C_2} = 214$  nm,  $N_1 = 6$ , and  $N_2 = 5$ . These structures show that the localization of homojunction PhC is not excessive and increasing the light absorption and emission of MoS<sub>2</sub> at the same time is difficult. When the light emission is strong, the light absorption is usually low, with an absorption of only approximately 0.2. When the pump light is obliquely incident and the pump and outgoing lights are on different sides, the absorption is the largest (approximately 0.33) but the outgoing light enhancement is low. If light emission is enhanced using longer PhC cycles than those used in the current study, the light absorption of MoS<sub>2</sub> will decrease. However, this case does not happen in h-PhC.

Finally, we discuss the effect of light localization and the feasibility of the experiment.

The effect of light localization: We used the Q value to judge the strength of light localization. The larger the Q value, the higher the light localization and light absorption and emission intensity of MoS<sub>2</sub>. However, the higher the Q value, the smaller the full width at half maximum of the spectral line and the narrower the absorption and PL spectra. Excessively narrow absorption and emission spectra are not conducive to practical application. Moreover, when the Q value is high, the microcavity affects the transition time of the exciton. Thus, in Optimizing the parameters, we choose  $N_1 \leq 7$  and  $N_2 \leq 7$ .

The feasibility of the experiment: PhC and 2D materials composite structures (particularly 2D materials-PhC microcavity) were created [14–16]. Compared with the existing structure, this structure only changes the lattice constant of the upper and lower reflectors of the PhC microcavity. Therefore, the experiment is completely achievable.

## Conclusion

We studied the effect of 1D h-PhC on the light absorption and emission of monolayer MoS<sub>2</sub> and obtained the analytical solution of light absorption and emission in 1D PhC-2D materials composite structures. h-PhC has more models of photon localization than common PhC, enhances the light emission and absorption of MoS<sub>2</sub> simultaneously, and increases the PL spectrum of MoS<sub>2</sub> by 2-3 orders of magnitude. When the pump light is obliquely incident and the pump and outgoing lights are on different sides of the h-PhC, it is easier to enhance the light absorption and emission of MoS<sub>2</sub> can be enhanced at the same time. The analytical solution can be used not only for light absorption and emission in h-PhC but also for the calculation of light emission and absorption of other 1D PhC-2D materials composite structures. This study has a promising prospect and important application value in 2D material-based optoelectronic devices.

## References

- [1] Wang, Q. H., Kalantar-Zadeh, K., Kis, A., Coleman, J. N. & Strano, M. S. Electronics and optoelectronics of two-dimensional transition metal dichalcogenides. *Nat. Nanotech.* **7**, 699–712 (2012).
- [2] Congxin, X. & Jingbo, L. Recent advances in optoelectronic properties and applications of two-dimensional metal chalcogenides. *Journal of Semiconductors* **37**, 051001 (2016). URL <http://stacks.iop.org/1674-4926/37/i=5/a=051001>.
- [3] Mak, K. F., Lee, C., Hone, J., Shan, J. & Heinz, T. F. Atomically thin MoS<sub>2</sub>: a new direct-gap semiconductor. *Phys. Rev. Lett.* **105**, 136805 (2010).
- [4] Splendiani, A. *et al.* Emerging photoluminescence in monolayer MoS<sub>2</sub>. *Nano Lett.* **10**, 1271–1275 (2010).
- [5] Lopez-Sanchez, O., Lembke, D., Kayci, M., Radenovic, A. & Kis, A. Ultrasensitive photodetectors based on monolayer MoS<sub>2</sub>. *Nat. Nanotech.* **8**, 497–501 (2013).
- [6] Guo, C. F., Sun, T., Cao, F., Liu, Q. & Ren, Z. Metallic nanostructures for light trapping in energy-harvesting devices. *Light: Science & Applications* **3**, e161 (2014).
- [7] Wang, F. *et al.* Progress on electronic and optoelectronic devices of 2d layered semiconducting materials. *Small* 1604298 (2017).
- [8] Lien, D.-H. *et al.* Engineering light outcoupling in 2d materials. *Nano Lett.* **15**, 1356–1361 (2015).
- [9] Butun, S., Tongay, S. & Aydin, K. Enhanced light emission from large-area monolayer mos2 using plasmonic nanodisc arrays. *Nano Lett.* **15**, 2700–2704 (2015).
- [10] Thongrattanasiri, S., Koppens, F. H. L. & de Abajo, F. J. G. Complete optical absorption in periodically patterned graphene. *Phys. Rev. Lett.* **108**, 047401 (2012).
- [11] Ferreira, A., Peres, N. M. R., Ribeiro, R. M. & Stauber, T. Graphene-based photodetector with two cavities. *Phys. Rev. B* **85**, 115438 (2012).
- [12] Ferreira, A. & Peres, N. M. R. Complete light absorption in graphene-metamaterial corrugated structures. *Phys. Rev. B* **86**, 205401 (2012).
- [13] Wang, W. *et al.* Enhanced absorption in two-dimensional materials via fano-resonant photonic crystals. *Appl. Phys. Lett.* **106**, 181104 (2015).
- [14] Furchi, M. *et al.* Microcavity-integrated graphene photodetector. *Nano Lett.* **12**, 2773–2777 (2012).

- [15] Engel, M. *et al.* Light-matter interaction in a microcavity-controlled graphene transistor. *Nature Communications* **3**, 906 (2012).
- [16] Sandhu, S., Yu, Z. & Fan, S. Detailed balance analysis and enhancement of open-circuit voltage in single-nanowire solar cells. *Nano Lett.* **14**, 1011–1015 (2014).
- [17] Zhang, Z. Z., Chang, K. & Peeters, F. M. Tuning of energy levels and optical properties of graphene quantum dots. *Phys. Rev. B* **77**, 235411 (2008).
- [18] Vincenti, M. A., de Ceglia, D., Grande, M., D’Orazio, A. & Scalora, M. Nonlinear control of absorption in one-dimensional photonic crystal with graphene-based defect. *Opt. Lett.* **38**, 3550–3553 (2013).
- [19] Guozhi, J., Peng, W., Yanbang, Z. & Kai, C. Localized surface plasmon enhanced photothermal conversion in bi2se3 topological insulator nanoflowers. *Sci Rep.* **6**, 25884 (2016).
- [20] Shuyuan, X. *et al.* Tunable light trapping and absorption enhancement with graphene ring arrays. *Phys. Chem. Chem. Phys.* **18**, 26661–26669 (2016).
- [21] Wu, Y.-B., Yang, W., Wang, T.-B., Deng, X.-H. & Liu, J.-T. Broadband perfect light trapping in the thinnest monolayer graphene-mos2 photovoltaic cell: the new application of spectrum-splitting structure. *Scientific Reports* **6**, 20955 (2016).
- [22] Zheng, J., Barton, R. A. & Englund, D. Broadband coherent absorption in chirped-planar-dielectric cavities for 2d-material-based photovoltaics and photodetectors. *ACS Photonics* **1**, 768–774 (2014).
- [23] Linshuang, L., Yue, Y., Hong, Y. & Liping, W. Optical absorption enhancement in monolayer mos2 using multi-order magnetic polaritons. *Journal of Quantitative Spectroscopy and Radiative Transfer* **200**, 198–205 (2017).
- [24] Zhao, C. X., Xu, W., Li, L. L., Zhang, C. & Peeters, F. M. Terahertz plasmon-polariton modes in graphene driven by electric field inside a fabry-perot cavity. *Journal of Applied Physics* **117**, 223104 (2015).
- [25] Zu, S. *et al.* Active control of plasmon-exciton coupling in mos2-ag hybrid nanostructures. *Advanced Optical Materials* **4**, 1463–1469 (2016).
- [26] Wang, M. *et al.* Plasmon-trion and plasmon-exciton resonance energy transfer from a single plasmonic nanoparticle to monolayer mos2. *Nanoscale* C7NR03909C (2017). URL <http://dx.doi.org/10.1039/C7NR03909C>.
- [27] Jeong, H. Y. *et al.* Optical gain in mos2 via coupling with nanostructured substrate: Fabry-perot interference and plasmonic excitation. *ACS Nano* **10**, 8192–8198 (2016).

- [28] Lu, H. *et al.* Nearly perfect absorption of light in monolayer molybdenum disulfide supported by multilayer structures. *Opt. Express* **25**, 21630–21636 (2017).
- [29] Yao, Z. *et al.* Tunable surface-plasmon-polariton-like modes based on graphene metamaterials in terahertz region. *Computational Materials Science* **117**, 544–548 (2016).
- [30] Ansari, N. & Mohebbi, E. Increasing optical absorption in one-dimensional photonic crystals including mos2 monolayer for photovoltaics applications. *Optical Materials* **62**, 152–158 (2016).
- [31] Wang, Z. *et al.* Giant photoluminescence enhancement in tungsten-diselenide-gold plasmonic hybrid structures. *Nature Communications* **7**, 11283 (2016).
- [32] Lee, K. C. J. *et al.* Plasmonic gold nanorods coverage influence on enhancement of the photoluminescence of two-dimensional mos2 monolayer. *Sci Rep.* **5**, 16374 (2015).
- [33] Sobhani, A. *et al.* Enhancing the photocurrent and photoluminescence of single crystal monolayer MoS<sub>2</sub> with resonant plasmonic nanoshells. *Appl. Phys. Lett.* **104**, 031112 (2014).
- [34] Gao, W. *et al.* Localized and continuous tuning of monolayer mos2 photoluminescence using a single shape-controlled ag nanoantenna. *Advanced Materials* **28**, 701–706 (2016).
- [35] Chen, H. *et al.* Manipulation of photoluminescence of two-dimensional mose2 by gold nanoantennas. *Sci Rep.* **6**, 22296 (2016).
- [36] Li, J. *et al.* Tuning the photo-response in monolayer mos2 by plasmonic nano-antenna. *Sci Rep.* **6**, 23626 (2016).
- [37] Galfsky, T. *et al.* Broadband enhancement of spontaneous emission in two-dimensional semiconductors using photonic hypercrystals. *Nano Lett.* **16**, 4940–4945 (2016).
- [38] Janisch, C. *et al.* Mos2 monolayers on nanocavities: enhancement in light-matter interaction. *2D Materials* **3**, 025017 (2016). URL <http://stacks.iop.org/2053-1583/3/i=2/a=025017>.
- [39] Zhu, Y. *et al.* Strongly enhanced photoluminescence in nanostructured monolayer mos2 by chemical vapor deposition. *Nanotechnology* **27**, 135706 (2016).
- [40] Noori, Y. J. *et al.* Photonic crystals for enhanced light extraction from 2d materials. *ACS Photonics* **3**, 2515–2520 (2016).
- [41] Lin, L.-L. & Li, Z.-Y. Interface states in photonic crystal heterostructures. *Phys. Rev. B* **63**, 033310 (2001).

- [42] Zhou, Y.-S., Gu, B.-Y. & Wang, F.-H. Guide modes in photonic crystal heterostructures composed of rotating non-circular air cylinders in two-dimensional lattices. *Journal of Physics: Condensed Matter* **15**, 4109–4118 (2003).
- [43] Palik, E. D. (ed.) *Handbook of Optical Constants of Solids* (Academic Press, Boston, 1985).
- [44] Klein, C. A. Room-temperature dispersion equations for cubic zinc sulfide. *Appl. Opt.* **25**, 1873–1875 (1986).
- [45] Yariv, A. & Yeh, P. (eds.) *Optical Waves in Crystals: Propagation and Control of Laser Radiation* (Wiley-Interscience,, New York, 1983).
- [46] Bendickson, J. M., Dowling, J. P. & Scalora, M. Analytic expressions for the electromagnetic mode density in finite, one-dimensional, photonic band-gap structures. *Phys. Rev. E* **53**, 4107 (1996).
- [47] Hofmann, S., Thomschke, M., Lüssem, B. & Leo, K. Top-emitting organic light-emitting diodes. *Opt. Express* **19**, A1250 (2011).
- [48] Deppe, D. G., Lei, C., Lin, C. C. & Huffaker, D. L. Spontaneous emission from planar microstructures. *Journal of Modern Optics* **41**, 325–344 (1994).
- [49] Yang, F.-F., Huang, Y.-L., Xiao, W.-B., Liu, J.-T. & Liu, N.-H. Control of absorption of monolayer mos2 thin-film transistor in one-dimensional defective photonic crystal. *Europhysics Letters* **112**, 37008 (2015).

## METHODS

The modified transfer matrix method is used to model the absorption of monolayer MoS<sub>2</sub> in the photonic crystal micro-cavity.

## Acknowledgements

This work was supported by the NSFC (Grant Nos. 11364033, 11764008, 61774168), Project of master’s excellent talent program in guizhou province (ZYRC[2014]008), and the Innovation Group Major Research Project of Department of Education in Guizhou Province (No. KY[2016]028).

## Author contributions

J.T.L. supervised the project, did the theoretical derivation and the numerical calculation, analyzed the results, and wrote the paper. T. H., W. Z. H., and W. J. B. analyzed of the results and wrote the paper. Z. Y. S. supervised the

project, analyzed the results, and wrote the paper. All authors discussed the results and commented on the manuscript.

*Conflict of Interest:* The authors declare no competing financial interest.